Seismic analysis of a petrochemistry petroleum coke plant using the F.E.M.

Mihai D.L. Ţălu, Ştefan D.L. Ţălu, Nicoleta Rizea and Marin Bică

***Abstract*—**In this paper are presented the experimental measurements and the theoretical studies concerning the fields of the spatial deformation and the stresses of a spatial structure for a petroleum coke plant as consequences of the variations of the vertical seismic loadings. These fields are calculated using the finite element method. The numerical results obtained from this study are usually used in the engineering practice to optimal design the spatial structure of petroleum coke plant or to predict and verify the effective stress of the structure. These methods permit a detailed study of fields with highly accuracy and for this reason are useful tool in the system designing.

***Keywords*—** Finite element method (F.E.M.), numerical simulation, petroleum coke plant, vertical seismic loadings.

I. Introduction

To provide a high coefficient of security in exploitation, the activity of design engineering of a spatial metal structure for a petroleum coke plant must take into consideration the important fields of deformations and stresses resulting as consequence of the seismic loadings [3], [15], [19].

It has been very common to use the FEM for structural dynamic calculations [3], [6]-[11], [16]-[19].

This research work presents in synthesis the systematic theoretical study through numerical simulation concerning the distributions of the deformations and stresses fields as consequence of the vertical seismic loadings applied to a petroleum coke plant. The plant subject to study is in exploitation from 1996, in a continuous regime work, on the petrochemistry platform of oil distillery Onesti, Romania [15].

Manuscript received September 5, 2008: Revised received November 12, 2008. This work was supported in part by the Romanian Ministry of Education, Research and Youth, through The National University Research Council, Grant PN–II–ID–PCE–2007–1, no. 440/1.10.2007, code ID_1107, 2007 - 2010.

Mihai D.L. Ţălu is with the University of Craiova, Romania. He is now with the Department of Applied Mechanics, Faculty of Mechanics, 165 Calea Bucuresti Street, Craiova, 200585 Romania (phone: +40-251-418-803; fax: +40-251-418-803; e-mail: mihai_talu@yahoo.com).

Ştefan D.L. Ţălu is with the Technical University of Cluj-Napoca, Romania. He is now with the Department of Descriptive Geometry and Engineering Graphics, Faculty of Mechanics, 103-105 B-dul Muncii Street, Cluj-Napoca, 400641 Romania (e-mail: stefan_ta@yahoo.com).

Nicoleta Rizea is with the Petroleum-Gas University of Ploiesti, Romania. She is now with the Department of General Mechanics Disciplines, 39 B-dul Bucuresti Street, Ploiesti, 100680 Romania (e-mail: nicoletarizea @yahoo.com).

Marin Bică is with the University of Craiova, Romania. He is now with the Department of Road Vehicles, Faculty of Mechanics, 165 Calea Bucuresti Street, Craiova, 200585 Romania (phone: +40-251-418-803; fax: +40-251-418-803; e-mail: mbica@mecanica.ucv.ro).

This plant has a production of 385 tones petroleum coke in 48 hours and in the constructive solution presented there is an ensemble with four identical section (Fig. 1) which work alternatively in cycles by 48 hours.

Seismic analysis of the petroleum coke plant is made with the computer modeling techniques that offer the optimum solutions in the seismic design. In reality the stress and the deformation fields owed by the loadings generated by the aleatory seismic phenomenon are simultaneous superposition over the other type of loadings that solicit the spatial metal structure of plant by mechanical and thermal cycle's types.

In this paper, an engineering seismic calculation method of petroleum coke plant will be introduced.

II. The Spatial Model of the Petroleum Coke Plant

The spatial model of petroleum coke plant it made using the Solid Works 2007 software [20], starting from the executions drawings of installation.

The constructive geometry of plant is complex and the sizes are big (28 x 6 x 6 m^3).

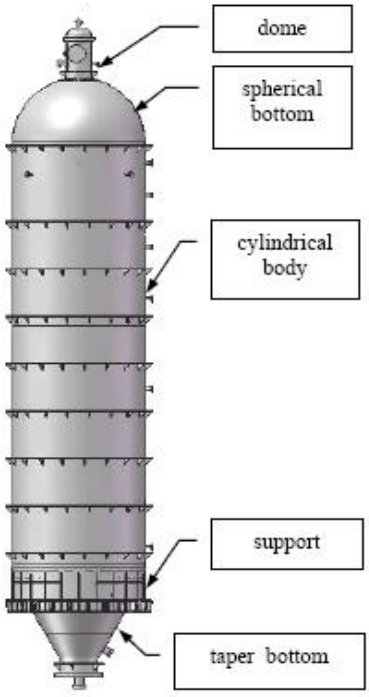

Fig. 1. The spatial model of the petroleum coke plant

Fig. 1 presents the 3D model from frontal view and on this model is noted the principal components.

A superior detail of the part of plant which includes the ensemble dome - spherical bottom is given in Fig. 2.

The middle section of plant represents the cylindrical body, Fig. 4. A detail view localized to the joint between the reinforcing rings, nervures and shell rings is shown in Fig. 3.

The 3D view and 3D section of the inferior section of plant is presented in Fig. 5 and Fig. 6.

These views represent the ensemble between taper bottom and support. A detail of support in shown in Fig. 7.

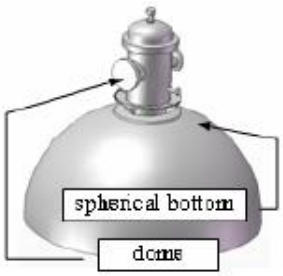

Fig. 2. The spatial model of ensemble spherical bottom – dome

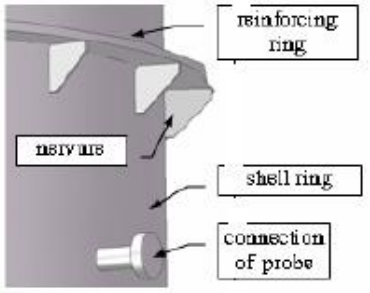

Fig. 3. A detail of joint between the reinforcing rings, nervures and shell rings

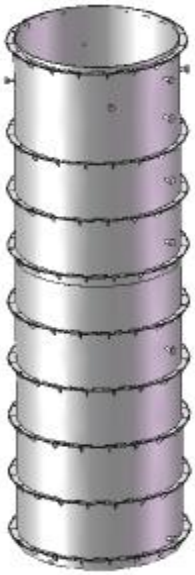

Fig. 4. The cylindrical body

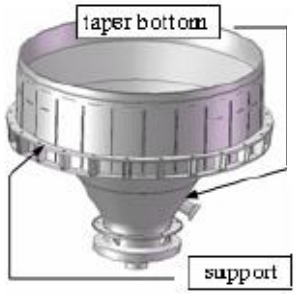

Fig. 5. The spatial model of the ensemble taper bottom – support

Fig. 6. The 3D section through the ensemble taper bottom - support

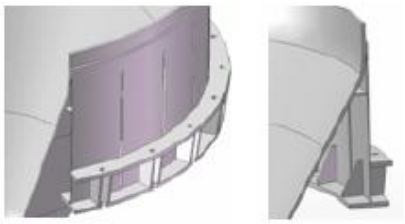

Fig. 7. The spatial details section through the support of petroleum coke plant

III. THE LOADINGS APPLIED TO THE PETROLEUM COKE PLANT

In paper [15] and [19] were detailed the loadings applied to the 3D metal structure of the petroleum coke plant. In fact these loadings have involved two components: the mechanical loading and the thermo - cyclical loading.

3.1. The mechanical loading

The mechanical loadings summing one component owed to the total force of weight of plant and one component owed to the vertical seismic loadings.

The total weight of plant force

The total force of weight of plant is equal with F_G = 542770.33 [daN] and represents the sum of five components marked with red arrows on Fig. 8.

The values of these forces are determined by experimental measurements:

- $F_{G\ gases}$, the force of gases weight accumulated into the dome; $F_{G\ gases}$ = 78 [daN];
- $F_{G\ C}$, the force of petroleum coke weight; is equal with $F_{G\ C}$ = 384770 [daN];
- $F_{G\ inst}$, the force of metal structure weight of plant; $F_{G\ inst}$ = 119266.40 [daN];

- $F_{G\,pl}$, the force of wall protection for corrosion of sulphur weight; $F_{G\,pl} = 9527.63$ [daN].
- $F_{G\ iz}$, the force of heat insulating wall weight; $F_{G\,iz} = 29128.30$ [daN].

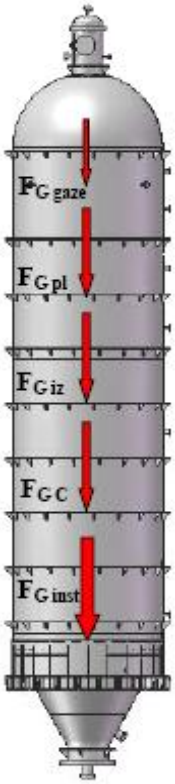

Fig. 8. The components of total force of weight for the petroleum coke plant

The vertical seismic loading force

In paper [15] is detailed the calculus of the effective value and distributions of vertical seismic loadings, applied to 3D metal structure of plant in according with recommendations of standards: S.T.R 8412-92 [28] and STAS 9315/1-80 [29].

The numerical simulations from this paper is made by considering the maximum values of the seismic loadings distributed to sections which initial was accepted to divide the plant. That's why in this study the structure of installation was divided in 56 equal sections, Fig. 9.

The plot of variation in sections of the maximum total seismic loading is presented in Fig. 10 and the plot of the gradient velocity of variation with h is given in Fig. 11.

The plot of the effective total loadings on sections is shown in Fig. 12.

The abbreviation used is next:

- $S_{max\ T}$, the whole maximum seismic force;
- G_{T}, the total weight of plant in work regime;
- $P_{ef\ T}$, the effective total loading force;

At level of plant support the $P_{ef\ T}$ have a maximum value equal with $P_{ef\ T\ max} = 652588$ [daN].

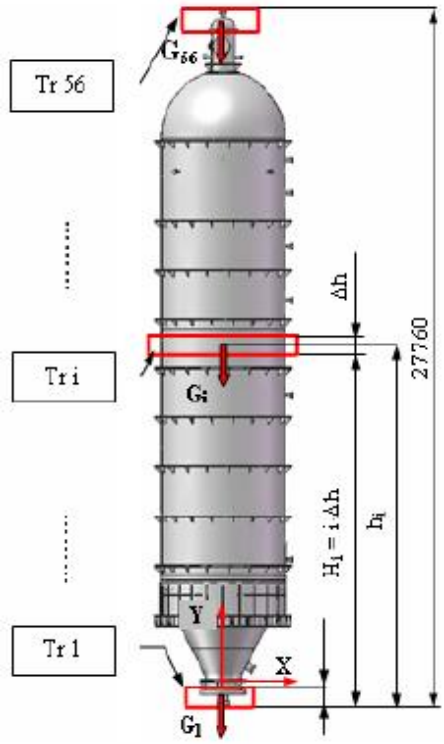

Fig. 9. The sketch of plant with sections in which are applied the vertical seismic loadings

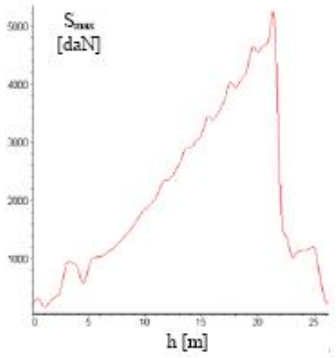

Fig. 10. The variation of the maximum total seismic loadings in installation

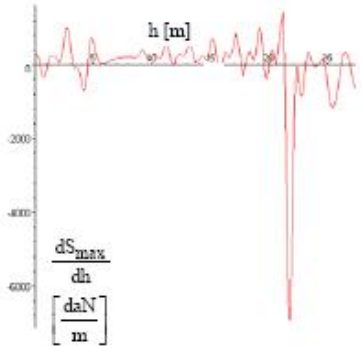

Fig. 11. The gradient velocity of variation with h for maximum total seismic loadings

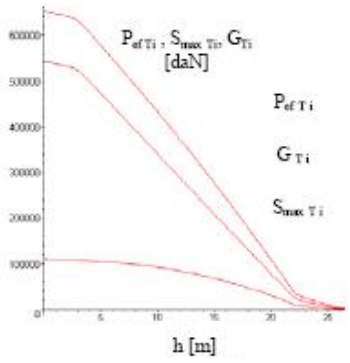

Fig. 12. The effective total loadings on sections

3.2. The cycling thermal loading

The production of the petroleum coke through the tardy method as consequence of technological process is accompanied by a cyclic variation of temperature T(h,P) which is transmitted to metal structure by the petroleum coke multiphase no homogeneous mixture formed during the transformation process of liquid petroleum in solid petroleum coke.

The temperature depends by the height of cote h and by the relative duration P that gives in % of the cycle carbon-producing.

As important consequence is generating the supplementary fields of deformations and stresses into the structure metal of plant.

In present it is difficult to estimate only the theoretically methods for the variations of T (h, P).

The realist solution of this problem is to practical solve through the experimental measurements and in this purpose scope are installed on the structure's walls of plant a number of nine thermocouples, Fig. 13 at levels specified in Table 1.

Table I. Tr_k (h_k).

Tr_k	h_k [mm]	Tr_k	h_k [mm]
Tr 1	0	Tr 6	12800
Tr 2	700	Tr 7	21650
Tr 3	3500	Tr 8	24500
Tr 4	7600	Tr 9	27500
Tr 5	9500		

By processing of the database delivered by these thermocouples along ten cycles of work, it was determined the 3D dependence T (P, h) [15] with plots given in Fig. 14, using the Maple 11 software [22].

Also the 2D plots of temperature dependences $T_k(P\_dat)\big|_{h_K=\text{constant}}$ and $\dfrac{d\left[T_k(P)\big|_{h_K=\text{constant}}\right]}{dP}$ with k = 1,…, 9 are given from Fig. 15 to Fig. 23.

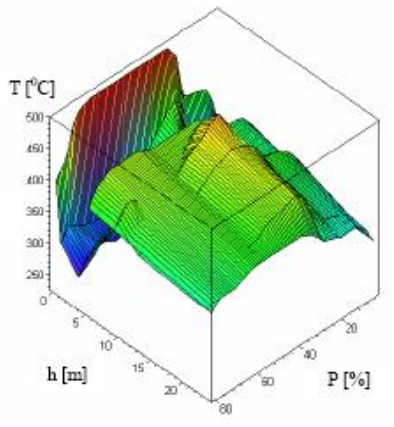

Fig. 14. The dependences T (P, h)

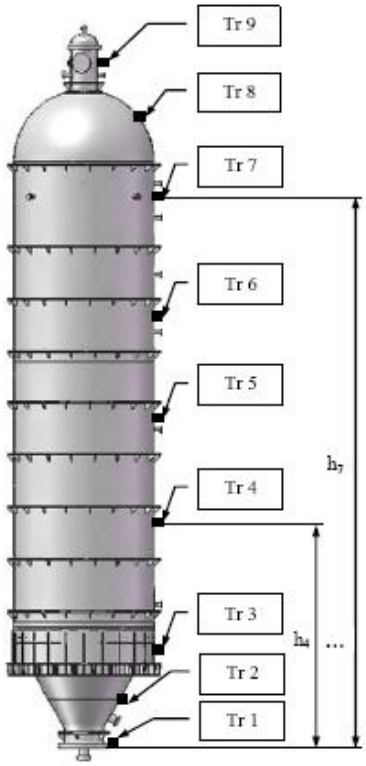

Fig. 13. The position of thermocouples

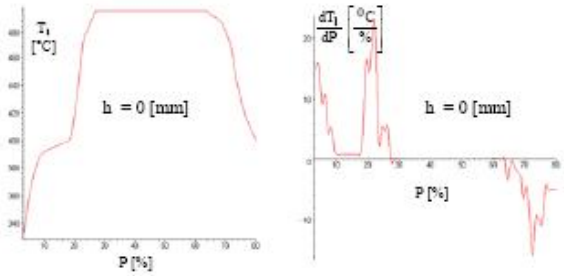

Fig. 15. Variations T(P) and $\dfrac{dT}{dP}$ at h = 0

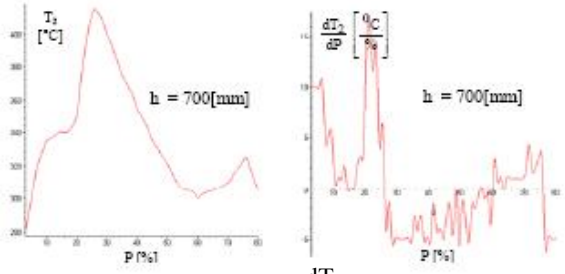

Fig. 16. Variations T(P) and $\frac{dT}{dP}$ at h = 700[mm]

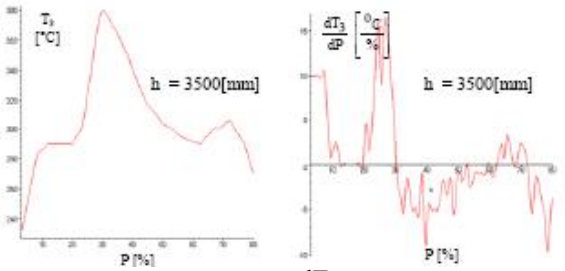

Fig. 17. Variations T(P) and $\frac{dT}{dP}$ at h = 3500[mm]

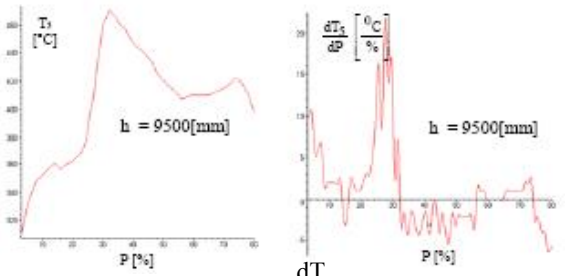

Fig. 18. Variations T(P) and $\frac{dT}{dP}$ at h = 9500[mm]

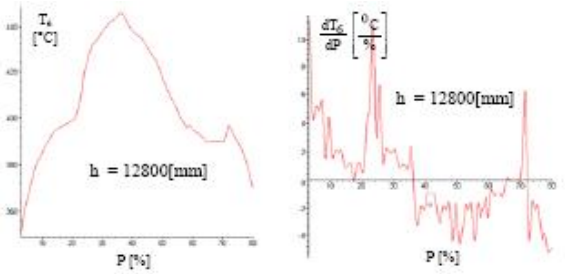

Fig. 19. Variations T(P) and $\frac{dT}{dP}$ at h = 12800[mm]

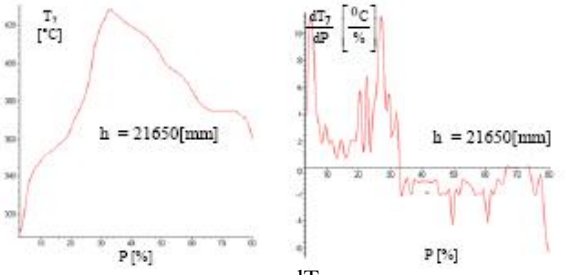

Fig. 20. Variations T(P) and $\frac{dT}{dP}$ at h = 21650[mm]

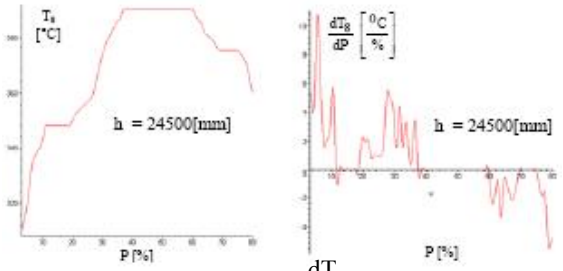

Fig. 21. Variations T(P) and $\frac{dT}{dP}$ at h = 24500[mm]

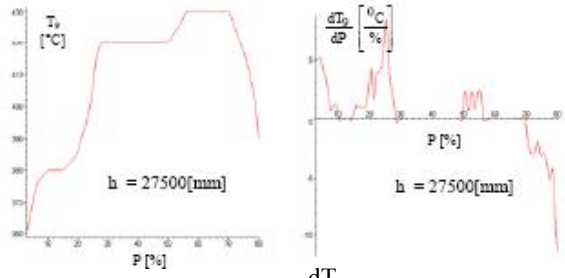

Fig. 22. Variations T(P) and $\frac{dT}{dP}$ at h = 27500[mm]

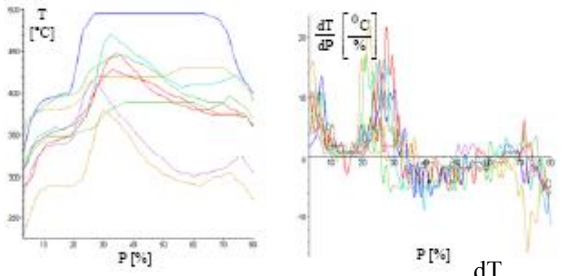

Fig. 23. Superposition of variations T(P) and $\frac{dT}{dP}$

The 2D plots of temperature dependences $T(h)\big|_{P=10\cdot K[\%]}$ and $\frac{T(h)}{dh}\Big|_{P=10\cdot K[\%]}$ with cu P = 10k, k = {1, 2, .. , 8 }are given in Fig. 24 to Fig. 31.

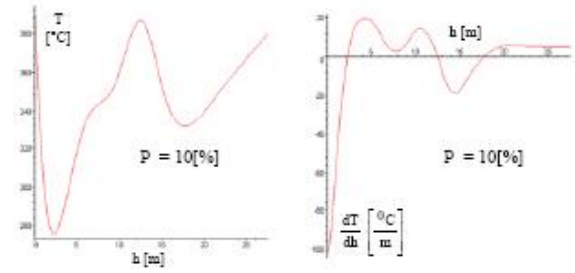

Fig. 24. Variations T(h) and $\frac{dT}{dh}$ at P = 10[%]

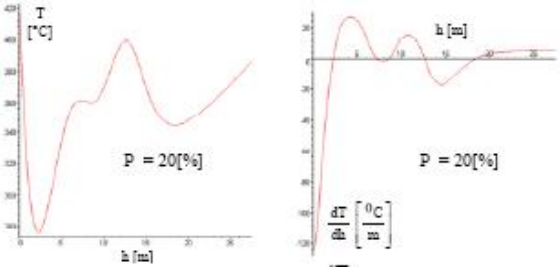

Fig. 25. Variations T(h) and $\frac{dT}{dh}$ at P = 20[%]

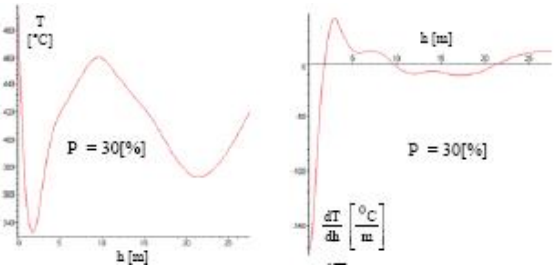

Fig. 26. Variations T(h) and $\frac{dT}{dh}$ at P = 30[%]

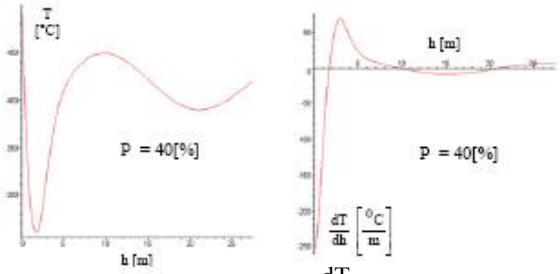

Fig. 27. Variations T(h) and $\frac{dT}{dh}$ at P = 40[%]

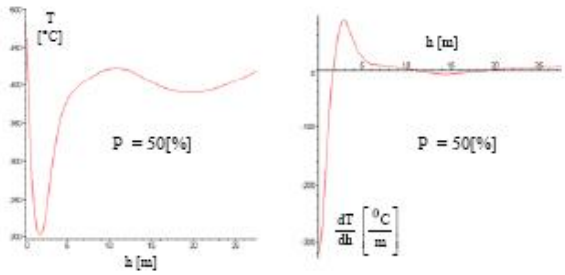

Fig. 28. Variations T(h) and $\frac{dT}{dh}$ at P = 50[%]

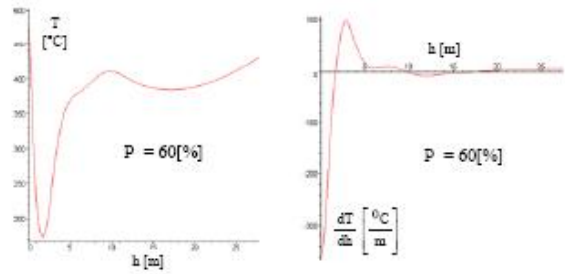

Fig. 29. Variations T(h) and $\frac{dT}{dh}$ at P = 60[%]

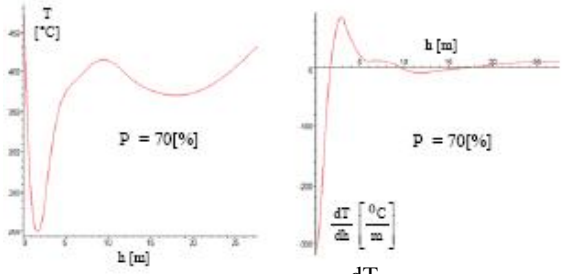

Fig. 30. Variations T(h) and $\frac{dT}{dh}$ at P = 70[%]

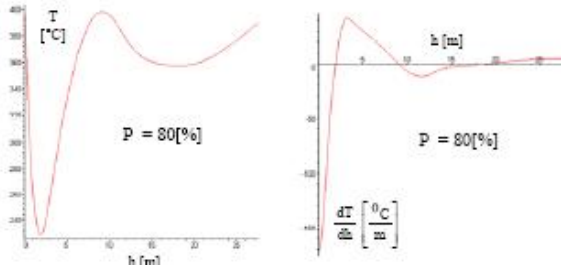

Fig. 31. Variations T(h) and $\frac{dT}{dh}$ at P = 80[%]

In present study the analysis with F.E.M. is made for a dependence of temperature T (h) at P = 60 %; Fig. 28 which corresponding to a complete process of carbon-producing cycle.

The most important constructive sections of petroleum coke plant with the proper loadings are presented in next figures.

The loadings for ensemble spherical bottom – dome

The mechanical loadings applied to ensemble spherical bottom – dome involves:

- the solicitation of the interior surface at pressure owed the gaseous generated during the technological process between h ∈ 22.5÷27.5 [m];
- the solicitation of the interior surface owed the weight of the stell 7AlCr130 used to protect the interior wall for the corrosion of sulphur;
- the solicitation of the exterior surface and a reinforcing rings owed the weight of the heat insulating wall;
- the solicitation of the whole ensemble of plant owed the gravitational attraction.

The thermal loading:

- the cyclic thermal solicitation of the interior surfaces for the whole ensemble owed the technological process of carbon-producing.

In Fig. 32 is localized the position of ensemble spherical bottom – dome on the plant and from Fig. 33 to Fig. 36 are given for this ensemble the plots of variations: T (h), S (h), G (h) and P (h).

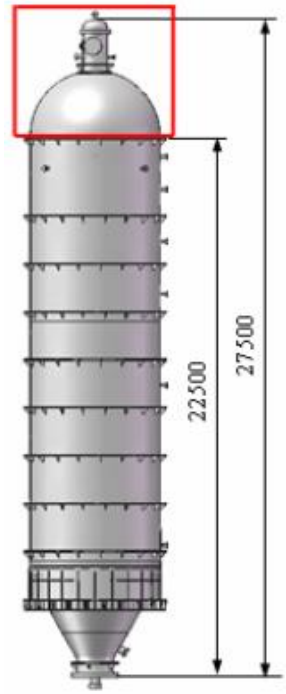

Fig. 32. The position of ensemble spherical bottom – dome on the plant

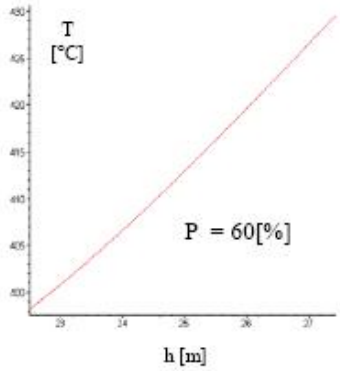

Fig. 33. The variation T (h)

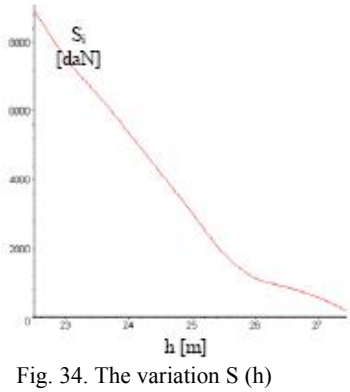

Fig. 34. The variation S (h)

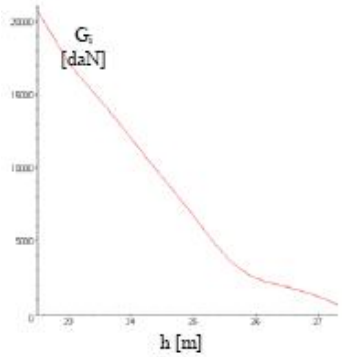

Fig. 35. The variation G (h)

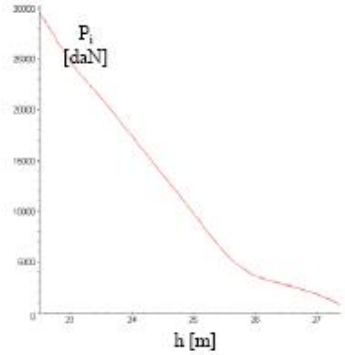

Fig. 36. The variation P (h)

The loadings for the cylindrical body

The mechanical loadings applied to the structure

- the solicitation of the interior surface corresponding to the nine shell ring owed the gaseous generating during the technological process (localized at surfaces of mixture fluid) between limits $h \in 21.65 \div 22.5$ [m];
- the solicitation of the interior surface owed the weight of gaseous generating;
- the solicitation of the interior surface owed the hydrostatic pressure of mixture fluid and of the gaseous weight between limits $h \in 4.75 \div 21.65$ [m];
- the solicitation of the interior surface owed the weight of the stell 7AlCr130 use to protect the interior wall for the corrosion of sulphur;
- the solicitation of the exterior surface and a reinforcing rings owed the weight of the heat insulating wall;
- the solicitation of the cylindrical body owed the gravitational attraction;

The thermal loading

- the cyclic thermal solicitation of the interior surfaces of cylindrical body owed the technological process of carbon-producing.

In Fig. 37 is localized the position of cylindrical body of the plant and from Fig. 38 to Fig. 42 are given for this ensemble the plots of variations for: p (h), T (h), S (h), G (h) and P (h).

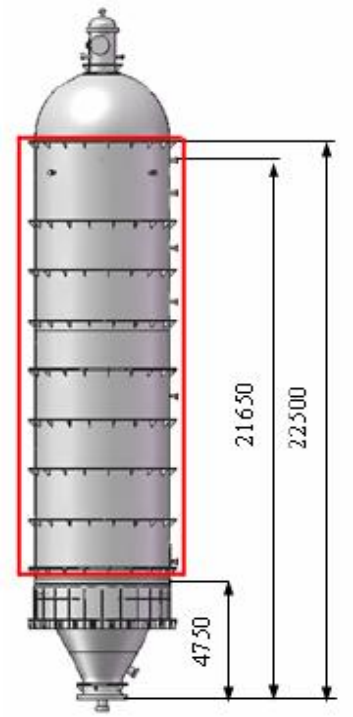

Fig. 37. The position of the cylindrical body of the plant

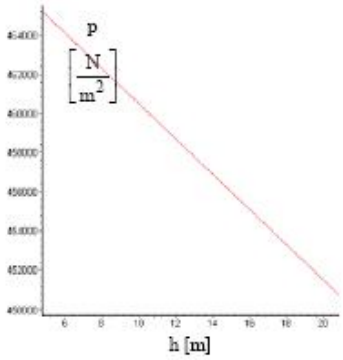

Fig. 38. The variation p (h)

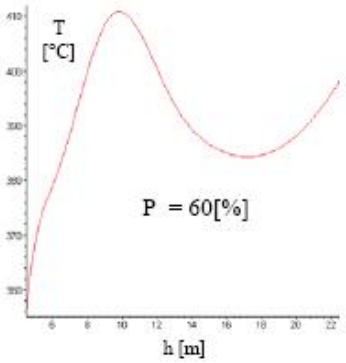

Fig. 39. The variation T (h)

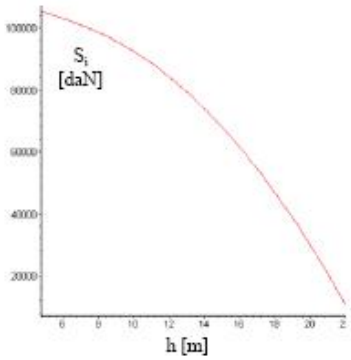

Fig. 40. The variation S (h)

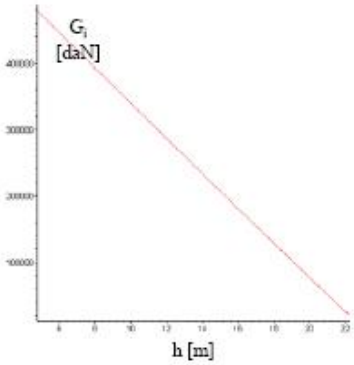

Fig. 41. The variation G (h)

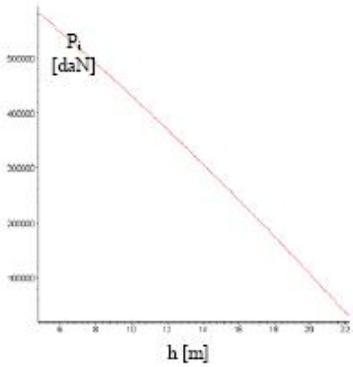

Fig. 42. The variation P (h)

The loadings applied to the taper bottom

The mechanical loadings are:

- the solicitation of the interior surface owed the hydrostatic pressure of mixture fluid between the limits $h \in 0 \div 4.75$ [m];
- the solicitation of the interior surface owed the weight of gaseous generating;
- the solicitation of the interior surface owed the weight of the stell 7AlCr130 use to protect the interior wall for the corrosion of sulphur;
- the solicitation of the exterior surface and a reinforcing rings owed the weight of the heat insulating wall;
- the solicitation owed the gravitational attraction.

The thermal loading :

- the cyclic thermal solicitation of the interior surfaces of taper bottom owed the technological process.

The loadings applied to the support of plant

The mechanical loadings are:

- the solicitation owed the gravitational attraction;

The thermal loading

- the cyclic thermal solicitation of the support through the conduction between the taper bottom and the support of the plant receiving at level of the common surfaces of contact.
- the permanent thermal solicitation through the convections at level of surface equal with the temperature of the ambient medium.

In Fig. 43 is localized the position of the ensemble taper bottom – support of plant and from Fig. 44 to Fig. 48 the plots: p (h), T (h), S (h), G (h) and P (h).

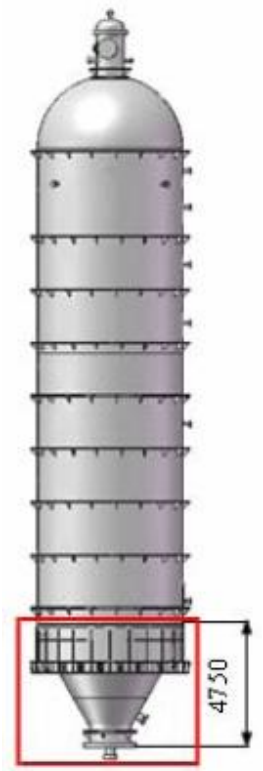

Fig. 43. The position of the ensemble taper bottom-support

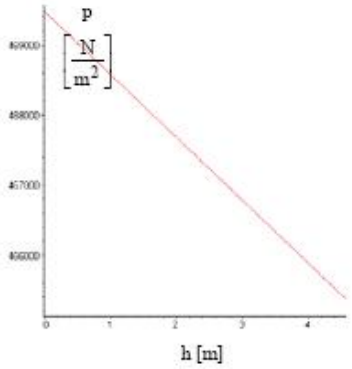

Fig. 44. The variation p (h)

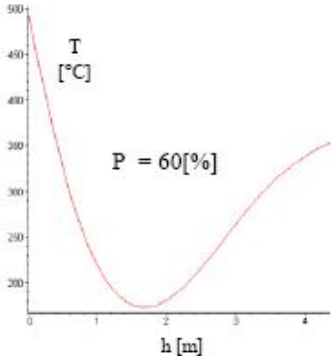

Fig. 45. The variation T (h)

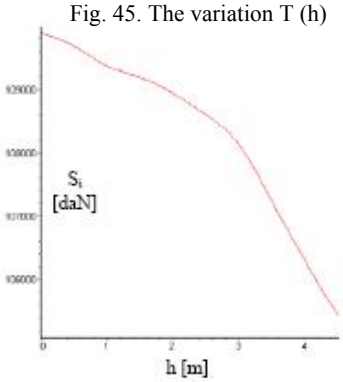

Fig. 46. The variation S (h)

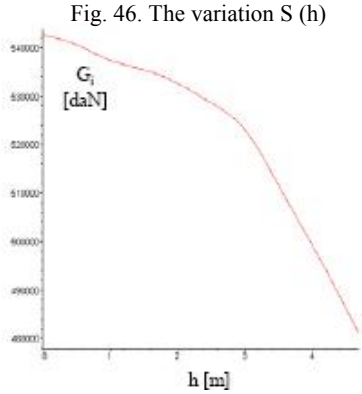

Fig. 47. The variation G (h)

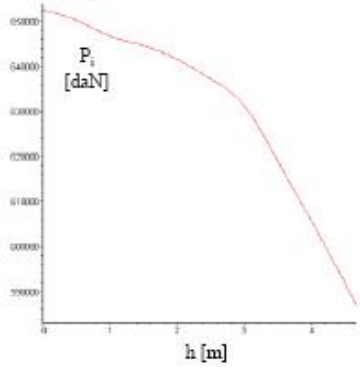

Fig. 48. The variation P (h)

IV. THE ANALYSIS WITH THE FEM OF THE STRESSES AND DEFORMATIONS FOR THE PLANT

The analysis with the F.E.M. is made using the Cosmos Works 2007 software [21]. We take into consideration the big building limits of the petroleum coke plant to keep the height accurate of the numerical simulation, the results are presented on every important component of installation

4.1. The F.E.M. analysis of the linear deformations fields

The fields of the linear deformations u_x, u_y, u_z and the resultant u_{rez} (Von Misses deformations) of the whole plant are given in Fig. 49 to Fig. 52.

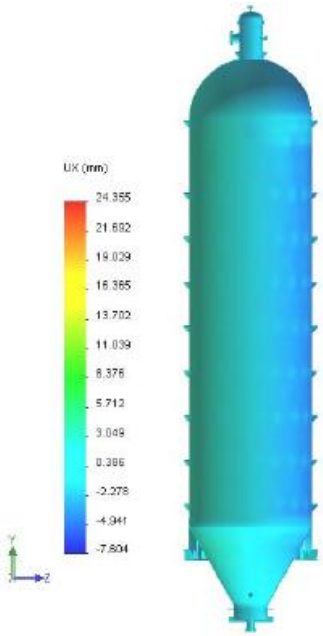

Fig. 49. The linear deformation u_x

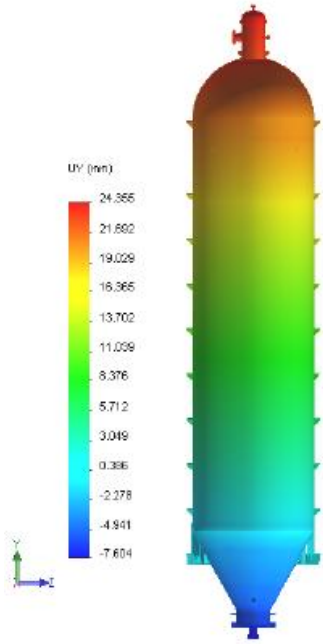

Fig. 50. The linear deformation u_y

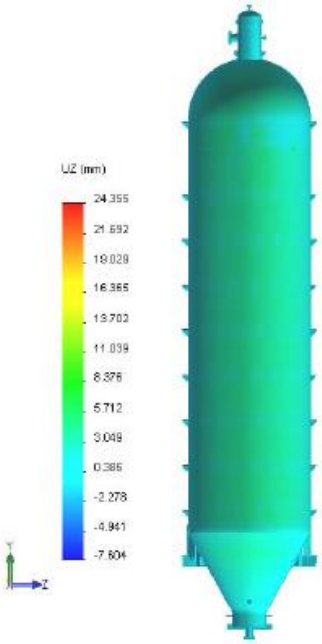

Fig. 51. The linear deformation u_z

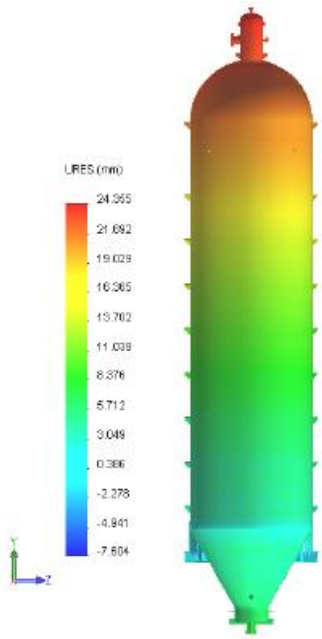

Fig. 52. The resultant linear deformation u_{rez}

4.2. The F.E.M. analysis of the stress fields

a) The F.E.M. analysis of the stress fields corresponding to the ensemble spherical bottom-dome

In Fig. 53 to Fig. 57 are presented the normal stress: σ_x, σ_y, σ_z, the resultant stress σ_{rez} and a detail of the resultant stress σ_{rez} at joint between dome and the spherical bottom.

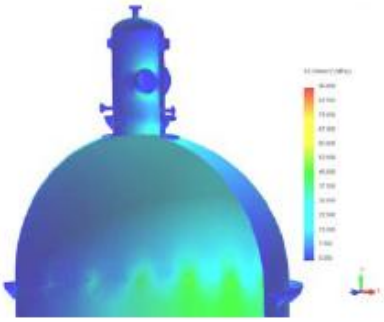

Fig. 53. The normal stress σ_x on dome and on the spherical bottom

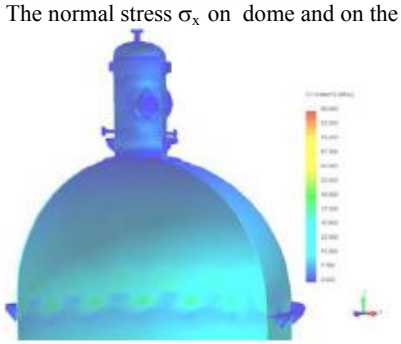

Fig. 54. The normal stress σ_y on dome and the spherical bottom

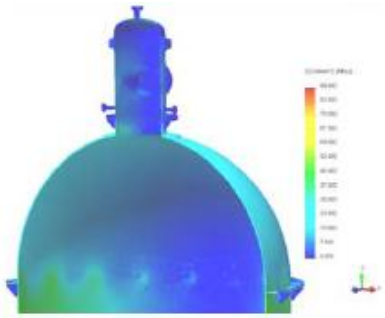

Fig. 55. The normal stress σ_z on dome and the spherical bottom

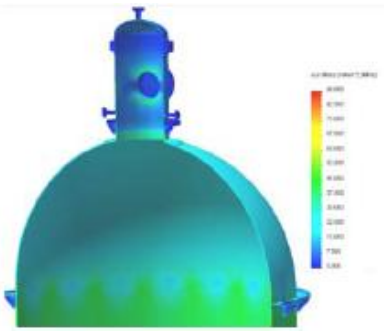

Fig. 56. The resultant stress σ_{rez} on dome and the spherical bottom

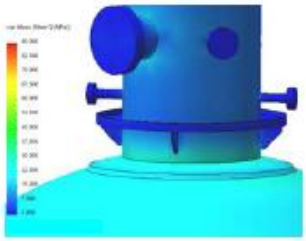

Fig. 57. A detail of resultant stress σ_{rez} at joint between dome and spherical bottom

b) The F.E.M. analysis of the stress fields corresponding to the cylindrical body

In Fig. 58 to Fig. 62 are given the fields of the normal stress: σ_x, σ_y, σ_z, the resultant stress σ_{rez} of cylindrical body and a detail of resultant stress σ_{rez} at joint between the reinforcing ring, the nervures and the shell ring.

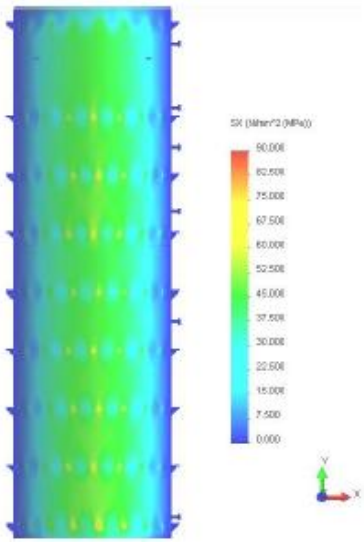

Fig. 58. The normal stress σ_x on cylindrical body

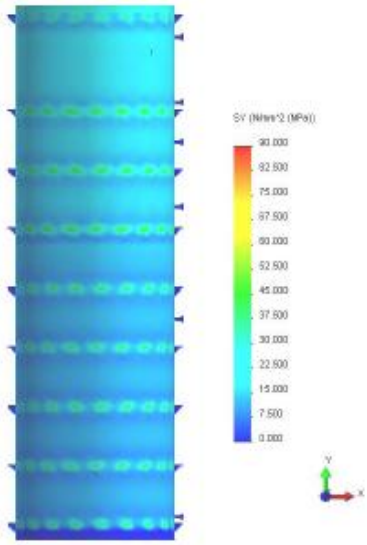

Fig. 59. The normal stress σ_y on cylindrical body

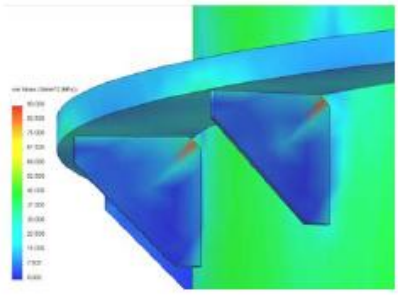

Fig. 62. A detail of resultant stress σ_{rez} of joint between the reinforcing ring, the nervures and the shell ring

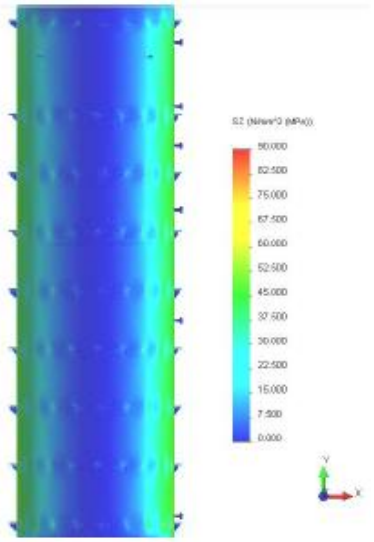

Fig. 60. The normal stress σ_z on cylindrical body

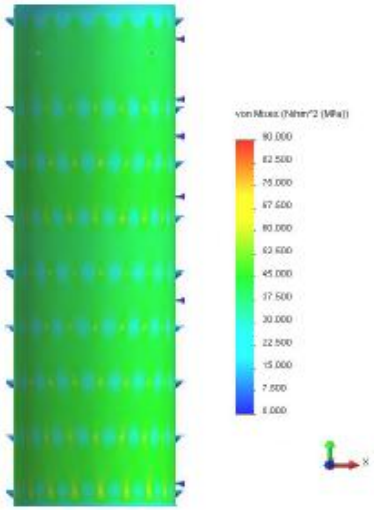

Fig. 61. The resultant stress σ_{rez} on cylindrical body

c) The F.E.M. analysis of the stress fields corresponding to the ensemble taper bottom - support of plant

In Fig. 63 to Fig. 66 are given the fields of the normal stress: σ_x , σ_y , σ_z and the resultant stress σ_{rez} of the ensemble taper bottom-support on section

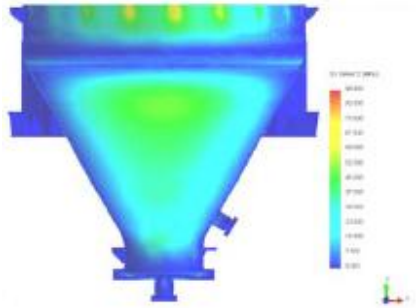

Fig. 63. The normal stress σ_x on the ensemble taper bottom-support

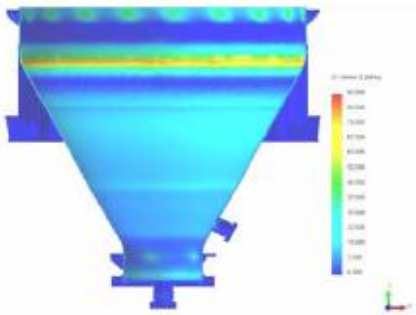

Fig. 64. The normal stress σ_y on the ensemble taper bottom-support

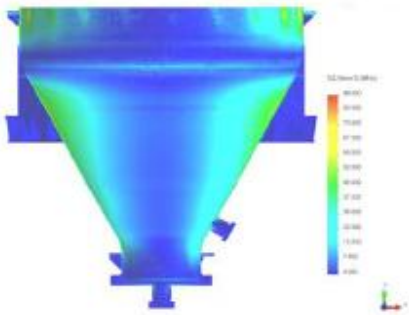

Fig. 65. The normal stress σ_z on the ensemble taper bottom-support

In Fig. 67 and Fig. 68 are given from different points of view the fields of the resultant stress σ_{rez} of the 3D ensemble taper bottom-support.

In Fig. 69 is presented a detail with numerical values of resultant stress of joint between cylindrical body and taper bottom.

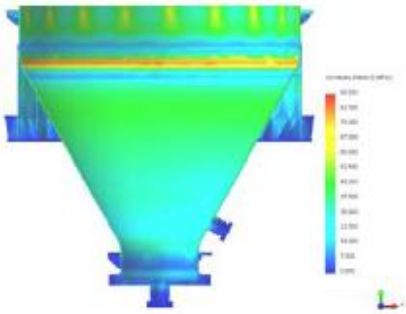

Fig. 66. The resultant stress σ_{rez} on the ensemble support- taper bottom

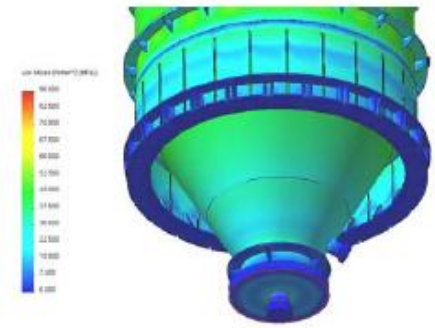

Fig. 67. The resultant stress σ_{rez} on the ensemble support- taper bottom

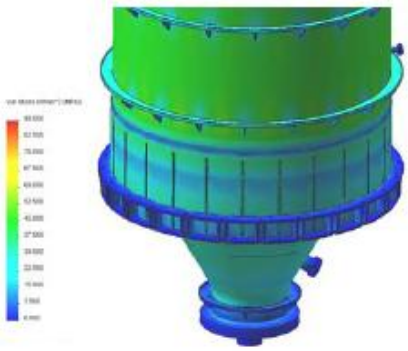

Fig. 68. The resultant stress σ_{rez} on the ensemble support- taper bottom

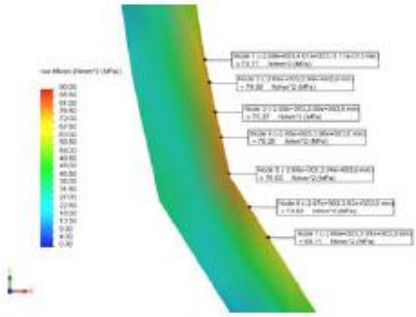

Fig. 69. The detail of resultant stress σ_{rez} at level of join between the cylindrical body and the taper bottom of installation

Other details with fields of the resultant stress σ_{rez} are presented in Fig. 70 and Fig. 71 concerning the detail 3D of join between the cylindrical body the taper bottom and the support plant and a detail 3D of the support of plant.

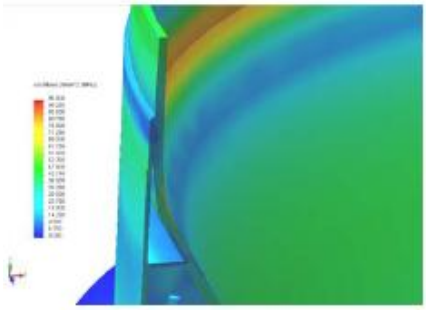

Fig. 70. The resultant stress σ_{rez} a detail 3D of joint between the cylindrical body on the ensemble taper bottom - support

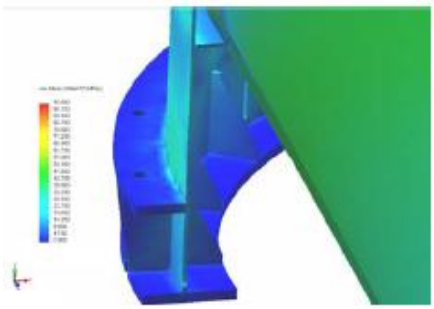

Fig. 71. The resultant stress σ_{rez} a detail of the support plant

V. CONCLUSIONS

The analysis with the Finite Element Method provides the spatial fields of deformations and stresses with high accuracy in optimum time.

The maximal value of the resultant deformations are equal with $u_{rez} = 25.35$ [mm], Fig. 51.

The resultant of stress on joint between the cylindrical body and the taper bottom have a maximum value equal with $\sigma_{rez} = 76.63$ [daN/mm^2], Fig. 69.

The maximum resultant stress on the spherical bottom is $\sigma_{rez} < 50$ [daN/mm^2], in concordance with Fig. 56.

At level of the cylindrical body $\sigma_{rez} < 60$ [daN/mm^2], Fig. 61 and at the support $\sigma_{rez} < 52$ [daN/mm^2], Fig. 71.

The loadings applied to the joint between the reinforcing rings, nervures and shell rings determinate a maximum $\sigma_{rez} = 72.31$ [daN/mm^2], Fig. 62.

The maximum effective values of stress are under admissible limit σ_{adm} /100000 cycles = 95 [daN/mm^2] corresponding to values give by STAS 2883/3-88 for alloy steel 16Mo5b which are used to build the plant structure.

REFERENCES

[1] Bockus S., "Solution of some differential equations of reversible and irreversible thermodynamics", *INTERNATIONAL JOURNAL of MECHANICS*, North Atlantic University Union Publishing House, issue 1, volume 1, 2007, pp. 10-14.

[2] Bratosin D., "Nonlinear effects in seismic base isolations", *WSEAS TRANSACTIONS on APPLIED and THEORETICAL MECHANICS*, WSEAS Press, issue 4, volume 3, April 2008, pp. 133-144.

[3] Calbureanu M., Albotă E., Malciu R., Lungu R., Calbureanu D., "Advanced computational concepts about projecting a multiple designs of self-supporting metallic structure using Finite Element Method in determination the buckling factor and running the stress analysis", *WSEAS TRANSACTIONS on APPLIED and THEORETICAL MECHANICS*, WSEAS Press, issue 5, volume 3, May 2008, pp. 186-195.

[4] Coffin L.F., "Predictive parameters and their applications to high temperature low cycle fatigue", in *Facture mechanics*, 1970.

[5] Djordjevic W., Elsabee F., "A survey and assement of major mechanical equipment capability during seismic events", *ASME-PVP* vol. 62, 1982, pp. 223-239.

[6] Dong Y., Redekop D., "Collapse analysis of liquid storage tanks under seismic action", *WSEAS TRANSACTIONS on APPLIED and THEORETICAL MECHANICS*, WSEAS Press, issue 3, volume 2, March 2007, pp. 79-85.

[7] Hughes T.J.R., "The finite element method linear static and dynamic finite element analysis", Prentice-hall, Inc, Englewood Cliffs, NJ, 1987.

[8] Kumarci K., Ziaie A., Koohikamali M., Kyioumarsi A., "Optimum shape in brick masonry arches under static and dynamic loads", *INTERNATIONAL JOURNAL of MATHEMATICS AND COMPUTERS IN SIMULATION*, North Atlantic University Union Publishing House, issue 2, volume 2, 2008, pp. 171-178.

[9] Leithner R., Zindler H., Hauschke A., "Optimization of the finite volume method source code by using polymorphism", *INTERNATIONAL JOURNAL of MATHEMATICS AND COMPUTERS IN SIMULATION*, North Atlantic University Union Publishing House, issue 3, volume 1, 2007, pp. 228 - 232.

[10] Leopa A., Nastac S., "Dynamical behavior of foundations in linear and nonlinear elastic characteristics hypothesis", *WSEAS TRANSACTIONS on APPLIED and THEORETICAL MECHANICS*, WSEAS Press, issue 4, volume 3, April 2008, pp. 145-154.

[11] Leopa A., Năstac S., "Experimental and theoretical analysis of the dynamical behaviour of the technological equipment foundation loads", *INTERNATIONAL JOURNAL of MECHANICS*, North Atlantic

University Union Publishing House, issue 4, volume 1, 2007, pp. 80-88
[12] Manson S.S., "Thermal stress and low-cycle fatigue", McGraw-Hill, 1974.
[13] Marciuc G.I., "Metode de analiză numerică", Ed. Academiei R.S.R., 1983.
[14] Mateiu H., "Fenomene de degradare la solicitări termomecanice", Teză de doctorat, I.S.I.M. Timisoara, 2002.
[15] Rizea N., "Contribuţii la calculul de fluaj şi oboseală al învelişurilor subţiri cu aplicaţie la aparatura petrochimică", Teză de doctorat, 2008, Universitatea Petrol–Gaze din Ploieşti, Romania.
[16] Roşca A., Roşca D., "Consideration concerning the static and dynamic stability of metallic bunker on environmental engineering", *WSEAS TRANSACTIONS on APPLIED and THEORETICAL MECHANICS,* WSEAS Press, issue 2, volume 3, February 2008, pp. 63-72.
[17] Ţălu M., Bolcu D., Ţălu Ş., Sipos A, "The dynamic flow air visualization around the petrochemistry petroleum coke plant", *Proceedings of the 9th WSEAS International Conference on AUTOMATION and INFORMATION (ICAI '08)*, Bucharest, Romania, June 24-26, 2008, WSEAS Press, pp. 164-169. ISSN: 1790-5117, ISBN: 978-960-6766-77-0.
[18] Ţălu M., Bică M., Albotă E., Ţălu Ş., "The dynamic visualization of the 3D thermal impression generated through the air friction with the petroleum coke plant structure", *Proceedings of the 5th WSEAS / IASME International Conference on ENGINEERING EDUCATION (EE '08)*, Heraklion, Greece, July 22-24, 2008, WSEAS Press, pp. 349-354, ISSN: 1790-2769, ISBN: 978-960-6766-86-2.
[19] Ţălu M., Bică M., Nanu Andrei Ghe., Albotă E., Ţălu Ş., Aurelian Ş., "Visualization of dynamic behaviour of a petrochemistry petroleum coke plant under verical various seismic loadings", *Proceedings of the 10th WSEAS International Conference on Mathematical and Computational Methods in Science and Engineering (MACMESE'08),* Bucharest, Romania, November 7-9, 2008, WSEAS Press, pp. 88-93, ISSN: 1790-2769, ISBN: 978-960-474-019-2.
[20] **** User guide Solid Works 2007 software.
[21] **** User guide CosmosWorks 2007 software.
[22] **** User guide Maple 11 software.
[23] **** Criteria for design of Elevated Temperature, class 1 Components in Section III, Division 1, of the ASME Boiler and Pressure Vessel Code ASME 2008
[24] ****ASM E Code. Case N-47: Design analysis of components in elevated temperature service edition 1999
[25] ****ASTM E 606 Constant amplitude low-cycle fatigue testing
[26] ****ASTM E 647 Standard test method for measurement of fatigue crack growth rates
[27] ****ASTM E 739-96 Statistical analysis of linear or linearized stress-life (S-N) and strain-life (ε-N) fatigue data
[28] **** S.T.R 8412-92**.**
[29] **** STAS 9315/1-80.
[30] **** STAS 2883/3-88.